C. R. Mecanique 347 (2019) 207–217

Contents lists available at ScienceDirect

Comptes Rendus Mecanique

www.sciencedirect.com

High-order shear theory for static analysis of functionally graded plates with porosities

Slimane Merdaci [a,*], Hakima Belghoul [b]

[a] Structures and Advanced Materials in Civil Engineering and Public Works Laboratory, University of Sidi Bel Abbes, Faculty of Technology, Civil Engineering and Public Works Department, Algeria
[b] Laboratoire de mécanique physique des matériaux (LMPM), Université Djillali-Liabès de Sidi Bel Abbes, Algeria

ARTICLE INFO

Article history:
Received 5 October 2018
Accepted 2 January 2019
Available online 28 January 2019

Keywords:
High-order theory
Functionally graded
Porosity
Plates

ABSTRACT

The bending responses of porous functionally graded (FG) thick rectangular plates are investigated according to a high-order shear deformation theory. Both the effect of shear strain and normal deformation are included in the present theory and so it does not need any shear correction factor. The equilibrium equations according to the porous FG plates are derived. The solution to the problem is derived by using Navier's technique. Numerical results have been reported and compared with those available in the open literature for non-porous plates. The effects of the exponent graded and porosity factors are investigated.

1. Introduction

Functionally graded materials (FGMs) are known for them tailor-made properties that are achieved through the continuous gradation of material phase from one surface to another. Due to FGMs being involved in the classification of composite materials, the material compositions of FGMs are assumed to vary smoothly and continuously throughout the gradient's directions. The earliest FGMs were introduced by Japanese scientists in the mid-1980s as ultra-high-temperature-resistant materials for aerospace applications. Recently, these materials have found other uses in electrical devices, energy transformation, biomedical engineering, optics, etc. [1]. At the introduction of FGMs, most of the essential concepts and information about the materials were largely unknown outside of Japan. However, in the manufacture of FGM, porosities may occur in the materials during the sintering process. This is due to the large difference in coagulation temperature between the components of the material [2]. Wattanasakulpong et al. [3] discussed the porosities that occur in lateral FGM samples made with a multistage sequential filtration technique. So, it is important to take under consideration the porosity effect when designing FG components under the effect of dynamic loadings.

Based on the open literature, it seems that many investigators have paid attention to the analysis of FGM structures with porosities. Most of these investigations are concerned with the vibration behavior of FG porous structures [4–28]. Additional researchers are restricted their attention to the buckling [29–38] or vibration and buckling [39–42] of many porous structures. Behravan Rad [43] presented the static response of porous multi-directional heterogeneous structures resting on the developed gradient elastic foundations.

* Corresponding author.
E-mail address: slimanem2016@gmail.com (S. Merdaci).

https://doi.org/10.1016/j.crme.2019.01.001
1631-0721/

In the past three decades, researches on plates have received great attention, and a variety of plate theories has been proposed, in which the plates are generally subjected to various types of mechanical loads. In particular, knowledge pertaining to bending is essential for optimal design of structures. For example, our numerical examples clearly show that, with a suitable volume fraction exponent "P" for FGM, one could achieve an optimal design for FGM plates.

It is worthwhile to present some developments in the plate theory. The first-order shear deformation theories (FSDPTs) based on Reissner [44] and Mindlin [45] accounted for the transverse shear effects by means of linear variation of in-plane displacements across the thickness. Since FSDPT violates the equilibrium conditions at the plate's top and bottom faces, the shear correction factors are needed to rectify the unrealistic variation of the shear strain/stress across the thickness. In order to overcome the limitations of FSDPT, higher-order shear deformation theories (PSDPTs) involving higher-order terms in Taylor's expansions of the displacements in the thickness coordinate were developed in Refs. [46–52]. A good review of these theories for the analysis of laminated composite plates is available in Refs. [53–57].

The objective of this article is to present the bending behavior of FG plates having porosities. The plate may be either perfectly porous homogeneous or has a perfect homogeneity shape depending on the values of the volume fraction of voids (porosity) or of the graded factors. The plate is assumed isotropic at any point within the plate, with its Young's modulus varying across its thickness in accord with a power law in terms of the volume fractions of the plate constituents while the Poisson's ratio remains constant. The present theory satisfies equilibrium conditions at the plate's top and bottom faces without using shear correction factors. A Navier solution is used to obtain closed-form solutions for simply supported FG plates. Several important aspects, i.e. aspect ratios, thickness ratios, exponent graded factor as well as porosity volume fraction, which affect deflections and stresses, are investigated.

2. Basic assumptions of the present plate theory

Consider a FG thick rectangular plate of length a, width b, and thickness h. The coordinate system is taken such that the x–y plane coincides with midplane of the plate. Let the FG plate be subjected to a transverse load $q(x, y)$. The plate is composed of a functionally graded material across the thickness direction. The assumptions of the present plate theory are as follows:

- the displacements are small in comparison with the plate thickness; therefore, the strains involved are infinitesimal;
- the transverse displacement w includes two components of bending w_b, and shear w_s; these components are functions of the coordinates x, y only,

$$w(x, y, z) = w_b(x, y) + w_s(x, y) \tag{1}$$

- the transverse normal stress σ_z is negligible in comparison with in-plane stresses σ_x and σ_y;
- the displacements u in the x-direction and v in the y-direction consist of extension, bending, and shear components,

$$U = u_0 + u_b + u_s, \qquad V = v_0 + v_b + v_s \tag{2}$$

The bending components u_b and v_b are assumed to be similar to the displacements given by the classical plate theory. Therefore, the expression for u_b and v_b can be given as

$$u_b = -z\frac{\partial w_b}{\partial x}, \qquad v_b = -z\frac{\partial w_b}{\partial y} \tag{3}$$

The shear components $\boldsymbol{u_s}$ and $\boldsymbol{v_s}$ give rise, in conjunction with $\boldsymbol{w_s}$ to the parabolic variations of the shear strains $\boldsymbol{\gamma_{xz}}$, $\boldsymbol{\gamma_{yz}}$, and hence to shear stresses $\boldsymbol{\tau_{xz}}$, $\boldsymbol{\tau_{yz}}$ through the thickness of the plate in such a way that shear stresses $\boldsymbol{\tau_{xz}}$, $\boldsymbol{\tau_{yz}}$ are zero at the top and bottom faces of the plate. Consequently, the expression for $\boldsymbol{u_s}$ and $\boldsymbol{v_s}$ can be given as

$$u_s = -f(z)\frac{\partial w_s}{\partial x}, \qquad v_s = -f(z)\frac{\partial w_s}{\partial y} \tag{4}$$

where

$$f(z) = z - \frac{h}{\pi}\sin\left(\frac{\pi z}{h}\right) \tag{5}$$

3. Kinematics

In the present analysis, the shear deformation plate theory is suitable for the displacements [60]:

$$\begin{aligned} u(x, y, z) &= u_0(x, y) - z\frac{\partial w_b}{\partial x} + f(z)\frac{\partial w_s}{\partial x} \\ v(x, y, z) &= v_0(x, y) - z\frac{\partial w_b}{\partial y} + f(z)\frac{\partial w_s}{\partial y} \\ w(x, y, z) &= w_b(x, y) + w_s(x, y) \end{aligned} \tag{6}$$

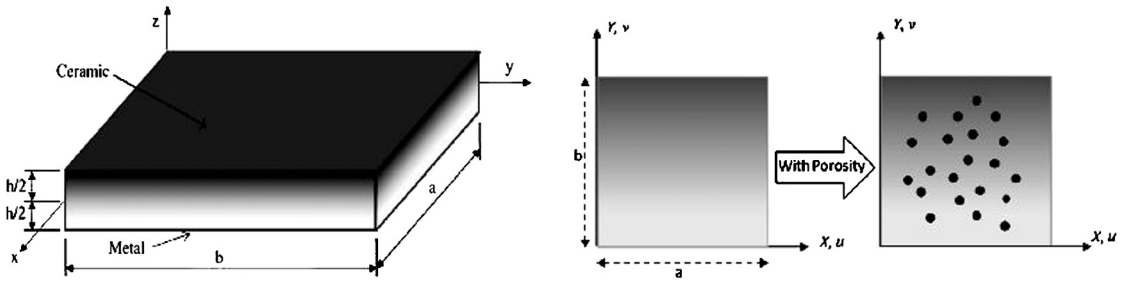

Fig. 1. Geometry and coordinates of the FG porous plate.

The strains associated with the displacements in Eq. (7) are

$$\begin{Bmatrix} \varepsilon_x \\ \varepsilon_y \\ \gamma_{xy} \end{Bmatrix} = \begin{Bmatrix} \varepsilon_x^0 \\ \varepsilon_y^0 \\ \gamma_{xy}^0 \end{Bmatrix} + z \begin{Bmatrix} k_x^b \\ k_y^b \\ k_{xy}^b \end{Bmatrix} + f(z) \begin{Bmatrix} k_x^s \\ k_y^s \\ k_{xy}^s \end{Bmatrix}$$
$$\begin{Bmatrix} \gamma_{yz} \\ \gamma_{xz} \end{Bmatrix} = g(z) \begin{Bmatrix} \gamma_{yz}^s \\ \gamma_{xz}^s \end{Bmatrix}, \quad \varepsilon_z = 0 \tag{7}$$

where

$$\begin{Bmatrix} \varepsilon_x^0 \\ \varepsilon_y^0 \\ \gamma_{xy}^0 \end{Bmatrix} = \begin{Bmatrix} \frac{\partial u_0}{\partial x} \\ \frac{\partial v_0}{\partial y} \\ \frac{\partial u_0}{\partial y} + \frac{\partial v_0}{\partial x} \end{Bmatrix}, \quad \begin{Bmatrix} k_x^b \\ k_y^b \\ k_{xy}^b \end{Bmatrix} = \begin{Bmatrix} -\frac{\partial^2 w_b}{\partial x^2} \\ -\frac{\partial^2 w_b}{\partial y^2} \\ -2\frac{\partial^2 w_b}{\partial x \partial y} \end{Bmatrix}, \quad \begin{Bmatrix} k_x^s \\ k_y^s \\ k_{xy}^s \end{Bmatrix} = \begin{Bmatrix} \frac{\partial^2 w_s}{\partial x^2} \\ \frac{\partial^2 w_s}{\partial y^2} \\ 2\frac{\partial^2 w_s}{\partial x \partial y} \end{Bmatrix}, \quad \begin{Bmatrix} \gamma_{yz}^s \\ \gamma_{xz}^s \end{Bmatrix} = \begin{Bmatrix} \frac{\partial w_s}{\partial y} \\ \frac{\partial w_s}{\partial x} \end{Bmatrix} \tag{8}$$

$$g(z) = 1 - f'(z) \tag{9a}$$

$$f'(z) = \frac{\mathrm{d}f(z)}{\mathrm{d}z} \tag{9b}$$

4. Constitutive equations

The plate is graded from aluminum (bottom) to alumina (top), as depicted in Fig. 1. The mechanical properties of FGM are determined from the volume fraction of the material constituents. Young's modulus E is assumed to be a function of the volume fraction of the constituent materials. Let the present plate be converted from lower to upper surfaces according to an exponential or polynomial law. We will consider firstly a non-homogeneous material with a porosity volume function α $(0 \leq \alpha \leq 1)$. In such a way, the efficient material properties, as Young's modulus, can be expressed as:

$$E = E_0 \mathrm{e}^{(\frac{1}{2} - \frac{z}{h})^P - \frac{2\alpha}{1-\alpha}} \tag{10}$$

where P $(P \geq 0)$ represents a factor that points out the material variation through the thickness. Note that the plate is perfectly porous homogeneous when k equals zero; it gets a perfect homogeneity shape when $k = \alpha = 0$. E/E_0 denotes the relative or reduced tensile modulus, with E being the effective tensile modulus of the porous material and E_0 is the tensile modulus of the homogeneous one, and α represents the volume fraction of voids (porosity). Eq. (10) yields $E = 0$ as $\alpha = 1$.

The functional relationship between $E(z)$ for the ceramic and metal FGM plate is assumed to be [58,59]:

$$E(z) = (E_c - E_m)V + E_m - (E_c + E_m)\frac{\alpha}{2}, \quad \text{and } V = \left(\frac{1}{2} - \frac{z}{h}\right)^p \tag{11}$$

where E_c and E_m are the corresponding properties of the ceramic and the metal, respectively, and P is the volume fraction exponent, which takes values greater than or equal to zero. The above power-law assumption reflects a simple rule of mixtures used to obtain the effective properties of the ceramic/metal plate. The rule of mixtures applies only to the thickness direction. Note that the volume fraction of the metal is high near the bottom surface of the plate, and that of the ceramic is high near the top surface. Furthermore, Eq. (10) indicates that the bottom surface of the plate $(z = -h/2)$ is metal, whereas the top surface $(z = h/2)$ of the plate is ceramic.

The stress–strain relations for a linear and isotropic elastic plate are written as

$$\begin{Bmatrix} \sigma_x \\ \sigma_y \\ \tau_{xy} \end{Bmatrix} = \begin{bmatrix} Q_{11} & Q_{12} & 0 \\ Q_{12} & Q_{22} & 0 \\ 0 & 0 & Q_{66} \end{bmatrix} \begin{Bmatrix} \varepsilon_x \\ \varepsilon_y \\ \gamma_{xy} \end{Bmatrix}$$
$$\begin{Bmatrix} \tau_{yz} \\ \tau_{zx} \end{Bmatrix} = \begin{bmatrix} Q_{44} & 0 \\ 0 & Q_{55} \end{bmatrix} \begin{Bmatrix} \gamma_{yz} \\ \gamma_{zx} \end{Bmatrix} \tag{12}$$

where (σ_x, σ_y, τ_{xy}, τ_{yz}, τ_{yx}) and (ε_x, ε_y, γ_{xy}, γ_{yz}, γ_{yx}) are the stress and strain components, respectively. Using the material properties defined in Eq. (8), the stiffness coefficients Q_{ij} can be expressed as

$$Q_{11} = Q_{22} = \frac{E(z)}{1-\nu^2}, \qquad Q_{12} = \frac{\nu E(z)}{1-\nu^2}, \qquad Q_{44} = Q_{55} = Q_{66} = \frac{E(z)}{2(1+\nu)} \tag{13}$$

5. Governing equations

The static equations can be obtained by using the principle of virtual displacements. It can be stated in its analytical form as

$$\int (\delta U + \delta V) = 0 \tag{14}$$

where δU is strain energy variation and δV is potential energy variation. The variation of the strain energy of the plate writes

$$\delta U = \int_{-h/2}^{h/2} \int_A [\sigma_x \delta\varepsilon_x + \sigma_y \delta\varepsilon_y + \tau_{xy}\delta\gamma_{xy} + \tau_{yz}\delta\gamma_{yz} + \tau_{xz}\delta\gamma_{xz}]\,\mathrm{d}A\,\mathrm{d}z \tag{15a}$$

$$= \int_A \left[N_x \delta\varepsilon_x^0 + N_y \delta\varepsilon_y^0 + N_{xy}\delta\varepsilon_{xy}^0 + M_x^{\mathrm{b}}\delta k_x^{\mathrm{b}} + M_y^{\mathrm{b}}\delta k_y^{\mathrm{b}} + M_{xy}^{\mathrm{b}}\delta k_{xy}^{\mathrm{b}} + M_x^{\mathrm{s}}\delta k_x^{\mathrm{s}} + M_y^{\mathrm{s}}\delta k_y^{\mathrm{s}} + M_{xy}^{\mathrm{s}}\delta k_{xy}^{\mathrm{s}} + S_{yz}^{\mathrm{s}}\delta\gamma_{yz}^{\mathrm{s}} + S_{xz}^{\mathrm{s}}\delta\gamma_{xz}^{\mathrm{s}}\right]\mathrm{d}A \tag{15b}$$

where A is the top surface, and the stress resultants N, M, and S are defined by:

$$\begin{Bmatrix} N_x, & N_y, & N_{xy} \\ M_x^{\mathrm{b}}, & M_y^{\mathrm{b}}, & M_{xy}^{\mathrm{b}} \\ M_x^{\mathrm{s}}, & M_y^{\mathrm{s}}, & M_{xy}^{\mathrm{s}} \end{Bmatrix} = \int_{-h/2}^{h/2} (\sigma_x, \sigma_y, \tau_{xy}) \begin{Bmatrix} 1 \\ z \\ f(z) \end{Bmatrix} \mathrm{d}z, \qquad \left(S_{xz}^{\mathrm{s}}, S_{yz}^{\mathrm{s}}\right) = \int_{-h/2}^{h/2} (\tau_{xz}, \tau_{yz})^{(n)} g(z)\,\mathrm{d}z \tag{16}$$

The variation of potential energy of the applied loads can be expressed as

$$\delta V = -\int_A q(\delta w_{\mathrm{b}} + \delta w_{\mathrm{s}})\,\mathrm{d}A \tag{17}$$

Substituting the expressions for δU and δV from Eq. (15) and Eq. (17) and integrating the displacement gradients by parts and setting the coefficients δu, δv, δw_{b}, and δw_{s} zero separately, one obtains the equilibrium equations associated with the present shear deformation theory,

$$\begin{aligned}
&\delta u : \frac{\partial N_x}{\partial x} + \frac{\partial N_{xy}}{\partial y} = 0 \\
&\delta v : \frac{\partial N_{xy}}{\partial x} + \frac{\partial N_y}{\partial y} = 0 \\
&\delta w_{\mathrm{b}} : \frac{\partial^2 M_x^{\mathrm{b}}}{\partial x^2} + 2\frac{\partial^2 M_{xy}^{\mathrm{b}}}{\partial x \partial y} + \frac{\partial^2 M_y^{\mathrm{b}}}{\partial y^2} + q = 0 \\
&\delta w_{\mathrm{s}} : \frac{\partial^2 M_x^{\mathrm{s}}}{\partial x^2} + 2\frac{\partial^2 M_{xy}^{\mathrm{s}}}{\partial x \partial y} + \frac{\partial^2 M_y^{\mathrm{s}}}{\partial y^2} + \frac{\partial S_{xz}^{\mathrm{s}}}{\partial x} + \frac{\partial S_{yz}^{\mathrm{s}}}{\partial y} + q = 0
\end{aligned} \tag{18}$$

By substituting Eq. (7) into Eq. (12) and integrating through the thickness of the plate, the stress resultants are given as

$$\begin{Bmatrix} N \\ M^{\mathrm{b}} \\ M^{\mathrm{s}} \end{Bmatrix} = \begin{bmatrix} A & B & B^{\mathrm{s}} \\ A & D & D^{\mathrm{s}} \\ B^{\mathrm{s}} & D^{\mathrm{s}} & H^{\mathrm{s}} \end{bmatrix} \begin{Bmatrix} \varepsilon \\ k^{\mathrm{b}} \\ k^{\mathrm{s}} \end{Bmatrix}, \qquad S = A^s \gamma \tag{19}$$

$$N = \{N_x, N_y, N_{xy}\}^{\mathrm{t}}, \qquad M^{\mathrm{b}} = \left\{M_x^{\mathrm{b}}, M_y^{\mathrm{b}}, M_{xy}^{\mathrm{b}}\right\}^{\mathrm{t}}, \qquad M^{\mathrm{s}} = \left\{M_x^{\mathrm{s}}, M_y^{\mathrm{s}}, M_{xy}^{\mathrm{s}}\right\}^{\mathrm{t}} \tag{20a}$$

$$\varepsilon = \left\{\varepsilon_x^0, \varepsilon_y^0, \gamma_{xy}^0\right\}^{\mathrm{t}}, \qquad k^{\mathrm{b}} = \left\{k_x^{\mathrm{b}}, k_y^{\mathrm{b}}, k_{xy}^{\mathrm{b}}\right\}^{\mathrm{t}}, \qquad k^{\mathrm{s}} = \left\{k_x^{\mathrm{s}}, k_y^{\mathrm{s}}, k_{xy}^{\mathrm{s}}\right\}^{\mathrm{t}} \tag{20b}$$

$$A = \begin{bmatrix} A_{11} & A_{12} & 0 \\ A_{12} & A_{22} & 0 \\ 0 & 0 & A_{66} \end{bmatrix}, \qquad B = \begin{bmatrix} B_{11} & B_{12} & 0 \\ B_{12} & B_{22} & 0 \\ 0 & 0 & B_{66} \end{bmatrix}, \qquad D = \begin{bmatrix} D_{11} & D_{12} & 0 \\ D_{12} & D_{22} & 0 \\ 0 & 0 & D_{66} \end{bmatrix} \tag{20c}$$

$$B^{s}=\begin{bmatrix} B^{s}_{11} & B^{s}_{12} & 0 \\ B^{s}_{12} & B^{s}_{22} & 0 \\ 0 & 0 & B^{s}_{66} \end{bmatrix},\qquad D^{s}=\begin{bmatrix} D^{s}_{11} & D^{s}_{12} & 0 \\ D^{s}_{12} & D^{s}_{22} & 0 \\ 0 & 0 & D^{s}_{66} \end{bmatrix},\qquad H^{s}=\begin{bmatrix} H^{s}_{11} & H^{s}_{12} & 0 \\ H^{s}_{12} & H^{s}_{22} & 0 \\ 0 & 0 & H^{s}_{66} \end{bmatrix} \tag{20d}$$

$$S=\left\{S^{s}_{xz}, S^{s}_{yz}\right\}^{t},\qquad \gamma=\{\gamma_{xz},\gamma_{yz}\}^{t},\qquad A^{s}=\begin{bmatrix} A^{s}_{44} & 0 \\ 0 & A^{s}_{55} \end{bmatrix} \tag{20e}$$

where A_{ij}, B_{ij}, etc. are the plate stiffness defined by

$$\begin{aligned} \{A_{ij},B_{ij},D_{ij}\}&=\int_{-h/2}^{h/2}\left(1,z,z^{2}\right)Q_{ij}\mathrm{d}z\quad (i,j=1,2,6)\\ \left\{B^{s}_{ij},D^{s}_{ij},H^{s}_{ij}\right\}&=\int_{-h/2}^{h/2}\left(f(z),zf(z),f^{2}(z)\right)Q_{ij}\mathrm{d}z\quad (i,j=1,2,6)\\ \left\{A^{s}_{ij}\right\}&=\int_{-h/2}^{h/2}\left(\left[g(z)\right]^{2}\right)Q_{ij}\mathrm{d}z,\quad (i,j=4,5) \end{aligned} \tag{21}$$

Substituting from Eq. (19) into Eq. (18), the equations of motion can be expressed in terms of displacements (δu, δv, δw_b, δw_s) as

$$A_{11}\frac{\partial^{2}u}{\partial x}+A_{66}\frac{\partial^{2}u}{\partial y^{2}}+(A_{12}+A_{66})\frac{\partial^{2}v}{\partial x\partial y}-B_{11}\frac{\partial^{3}w_b}{\partial x^{3}}-(B_{12}+2B_{66})\frac{\partial^{3}w_b}{\partial x\partial y^{2}}-\left(B^{s}_{12}+2B^{s}_{66}\right)\frac{\partial^{3}w_s}{\partial x\partial y^{2}}-B^{s}_{11}\frac{\partial^{3}w_s}{\partial x^{3}}=0 \tag{22a}$$

$$A_{22}\frac{\partial^{2}v}{\partial y^{2}}+A_{66}\frac{\partial^{2}v}{\partial y^{2}}+(A_{12}+A_{66})\frac{\partial^{2}u}{\partial x\partial y}-B_{22}\frac{\partial^{3}w_b}{\partial y^{3}}-(B_{12}+2B_{66})\frac{\partial^{3}w_b}{\partial x^{2}\partial y}-\left(B^{s}_{12}+2B^{s}_{66}\right)\frac{\partial^{3}w_s}{\partial x^{2}\partial y}-B^{s}_{22}\frac{\partial^{3}w_s}{\partial y^{3}}=0 \tag{22b}$$

$$\begin{aligned} &B_{11}\frac{\partial^{3}u}{\partial x^{3}}+(B_{12}+2B_{66})\frac{\partial^{3}u}{\partial x\partial y^{2}}+(B_{12}+2B_{66})\frac{\partial^{3}v}{\partial x^{2}\partial y}+B_{22}\frac{\partial^{3}v}{\partial y^{3}}-D_{11}\frac{\partial^{4}w_b}{\partial x^{4}}-2(D_{12}+2D_{66})\frac{\partial^{4}w_b}{\partial x^{2}\partial y^{2}}\\ &-D_{22}\frac{\partial^{4}w_b}{\partial y^{4}}-D^{s}_{11}\frac{\partial^{4}w_s}{\partial x^{4}}-2\left(D^{s}_{12}+2D^{s}_{66}\right)\frac{\partial^{4}w_s}{\partial x^{2}\partial y^{2}}-D^{s}_{22}\frac{\partial^{4}w_s}{\partial y^{4}}+q=0 \end{aligned} \tag{22c}$$

$$\begin{aligned} &B^{s}_{11}\frac{\partial^{3}u}{\partial x^{3}}+\left(B^{s}_{12}+2B^{s}_{66}\right)\frac{\partial^{3}u}{\partial x\partial y^{2}}+\left(B^{s}_{12}+2B^{s}_{66}\right)\frac{\partial^{3}v}{\partial x^{2}\partial y}+B^{s}_{22}\frac{\partial^{3}v}{\partial y^{3}}-D^{s}_{11}\frac{\partial^{4}w_b}{\partial x^{4}}-2\left(D^{s}_{12}+2D^{s}_{66}\right)\frac{\partial^{4}w_b}{\partial x^{2}\partial y^{2}}\\ &-D^{s}_{22}\frac{\partial^{4}w_b}{\partial y^{4}}-H^{s}_{11}\frac{\partial^{4}w_s}{\partial x^{4}}-2\left(H^{s}_{12}+2H^{s}_{66}\right)\frac{\partial^{4}w_s}{\partial x^{2}\partial y^{2}}-H^{s}_{22}\frac{\partial^{4}w_s}{\partial y^{4}}+A^{s}_{55}\frac{\partial^{2}w_s}{\partial x^{2}}+A^{s}_{44}\frac{\partial^{2}w_s}{\partial y^{2}}+q=0 \end{aligned} \tag{22d}$$

6. Analytical solutions for FG plates

Rectangular plates are generally classified according to the type of support used. This paper is concerned with the exact solution to Eqs. (22a) and (22d) for a simply supported FG plate. The following boundary conditions are imposed at the side edges:

$$v_0=w_b=w_s=0,\qquad \frac{\partial w_b}{\partial y}=\frac{\partial w_s}{\partial y}=0,\qquad N_x=0,\ \text{and}\ M^{b}_{x}=M^{s}_{x}=0\ \text{and}\ x=0 \tag{23a}$$

$$u_0=w_b=w_s=0,\qquad \frac{\partial w_b}{\partial x}=\frac{\partial w_s}{\partial x}=0,\qquad N_y=0,\ \text{and}\ M^{b}_{y}=M^{s}_{y}=0\ \text{and}\ y=0 \tag{23b}$$

The external force according to Navier's solution can be expressed as

$$q(x,y)=\sum_{m=1}^{\infty}\sum_{n=1}^{\infty}q_{mn}\sin(\lambda x)\sin(\mu y) \tag{24}$$

where $\lambda=m\pi/a$ and $\mu=n\pi/b$, m and n are mode numbers. For the case of a sinusoidally distributed load, we have

$$m=n=1\quad\text{and}\quad q_{11}=q_0 \tag{25}$$

where q_0 represents the intensity of the load at the plate's center.

Table 1
Displacement models.

Model	Theory	Unknown variables
FSDPT	First-order shear deformation theory [62]	5
PSDPT	Parabolic shear deformation theory [49]	5
SSDPT	Sinusoidal shear deformation plate theory [61]	5
Present	Present higher-order shear deformation theory	4

Following the Navier solution procedure, we assume the following form of solution for (u, v, w_b, w_s), which satisfies the boundary conditions given in Eq. (21)

$$\begin{Bmatrix} u \\ v \\ w_b \\ w_s \end{Bmatrix} = \begin{Bmatrix} U_{mn}\cos(\lambda x)\sin(\mu y) \\ V_{mn}\sin(\lambda x)\cos(\mu y) \\ W_{bmn}\sin(\lambda x)\sin(\mu y) \\ W_{smn}\sin(\lambda x)\sin(\mu y) \end{Bmatrix} \tag{26}$$

where U_{mn}, V_{mn}, W_{bmn}, and W_{smn} are arbitrary parameters. Eq. (15), in combination with Eq. (18), can be combined into a system of first-order equations as:

$$[K]\{\Delta\} = \{F\} \tag{27}$$

where $\{\Delta\}$ and $\{F\}$ denote the columns

$$\{\Delta\}^{\mathrm{T}} = \{U_{mn}, V_{mn}, W_{bmn}, W_{smn}\}, \quad \text{and } \{F\}^{\mathrm{T}} = \{0, 0, -q_{mn}, -q_{mn}\} \tag{28}$$

$$[K] = \begin{bmatrix} a_{11} & a_{12} & a_{13} & a_{14} \\ a_{12} & a_{22} & a_{23} & a_{24} \\ a_{13} & a_{23} & a_{33} & a_{34} \\ a_{14} & a_{24} & a_{34} & a_{44} \end{bmatrix} \tag{29}$$

and the elements $a_{ij} = a_{ji}$ of the coefficient matrix $[K]$. The elements of the symmetric matrix $[K]$ presented in Eq. (27) are given by

$$\begin{aligned}
a_{11} &= -\left(A_{11}\lambda^2 + A_{66}\mu^2\right) \\
a_{12} &= -\lambda\mu(A_{12} + A_{66}) \\
a_{13} &= \lambda\left[B_{11}\lambda^2 + (B_{12} + 2B_{66})\mu^2\right] \\
a_{14} &= \lambda\left[B^s_{11}\lambda^2 + \left(B^s_{12} + 2B^s_{66}\right)\mu^2\right] \\
a_{22} &= -\left(A_{66}\lambda^2 + A_{22}\mu^2\right) \\
a_{23} &= \mu\left[(B_{12} + 2B_{66})\lambda^2 + B_{22}\mu^2\right] \\
a_{24} &= \mu\left[\left(B^s_{12} + 2B^s_{66}\right)\lambda^2 + B^s_{22}\mu^2\right] \\
a_{33} &= -\left(D_{11}\lambda^4 + 2(D_{12} + 2D_{66})\lambda^2\mu^2 + D_{22}\mu^4\right) \\
a_{34} &= -\left(D^s_{11}\lambda^4 + 2\left(D^s_{12} + 2D^s_{66}\right)\lambda^2\mu^2 + D^s_{22}\mu^4\right) \\
a_{44} &= -\left(H^s_{11}\lambda^4 + 2\left(H^s_{12} + 2H^s_{66}\right)\lambda^2\mu^2 + H^s_{22}\mu^4 + A^s_{55}\lambda^2 + A^s_{44}\mu^2\right)
\end{aligned} \tag{30}$$

7. Numerical results and discussions

In this section, the present theory is applied to the static analysis of FG plates. The Poisson ratio is fixed at $\nu = 0.3$, and comparisons are made with available solutions. The different modes of displacement are presented in Table 1; a comparison with the numerical case studies is used to check the accuracy of the present analysis. The FG plate is supposed to be aluminum and alumina with the following material properties:

- metal (aluminum, Al): $E_m = 70 \cdot 10^9$ N/m^2; $\nu = 0.3$
- ceramic (alumina, Al_2O_3): $E_c = 380 \cdot 10^9$ N/m^2; $\nu = 0.3$.

The various non-dimensional parameters used are: $\overline{w} = \frac{10hE_0}{a^2q_0}w(\frac{a}{2}, \frac{b}{2})$, $\overline{\sigma}_x = \frac{10h^2}{a^2q_0}\sigma_x(\frac{a}{2}, \frac{b}{2}, \frac{h}{2})$, $\overline{\tau}_{xz} = \frac{h}{aq_0}\tau_{xz}(0, \frac{b}{2}, 0)$, thickness coordinate $\overline{z} = z/\mathbf{h}$.

Table 2
Comparative study of deflections and dimensionless axial stress of FG plate for different volume fraction values and porosity coefficient $\alpha = 0$.

Theory	P	$\overline{w}$	$\overline{\sigma}_x$	$\overline{\tau}_{xz}$
FSDPT [62]	Ceramic	0.07791	1.97576	0.15915
PSDPT [49]		0.07791	1.99432	0.23857
SSDPT [61]		0.07790	1.99550	0.24618
Present		0.08122	1.99550	0.24618
FSDPT [62]	1	0.19609	0.93765	0.26880
PSDPT [49]		0.19604	0.94370	0.33433
SSDPT [61]		0.19604	0.94407	0.34103
Present		0.19703	0.94407	0.34103
FSDPT [62]	2	0.28661	1.36934	0.34892
PSDPT [49]		0.28490	1.37662	0.40919
SSDPT [61]		0.28479	1.37702	0.41426
Present		0.28479	1.37702	0.41426
FSDPT [62]	3	0.33851	1.61758	0.41003
PSDPT [49]		0.33624	1.62552	0.47133
SSDPT [61]		0.33606	1.62591	0.47502
Present		0.33606	1.62591	0.47502
FSDPT [62]	4	0.36738	1.75385	0.45817
PSDPT [49]		0.36474	1.76229	0.52541
SSDPT [61]		0.36452	1.76267	0.52827
Present		0.36452	1.76267	0.52827
FSDPT [62]	5	0.38402	1.83097	1.83097
PSDPT [49]		0.38116	1.83989	0.57337
SSDPT [61]		0.38090	1.84026	0.57591
Present		0.38090	1.84026	0.57591
FSDPT [62]	10	0.40768	1.94564	1.94564
PSDPT [49]		0.40799	1.95075	0.69891
SSDPT [61]		0.40790	1.95096	0.70450
Present		0.40703	1.95703	0.75376
FSDPT [62]	Metal	0.41919	1.97576	1.97576
PSDPT [49]		0.42164	1.98354	0.19984
SSDPT [61]		0.42172	1.98392	0.20359
Present		0.42290	1.99550	0.24618

As a first example, consider the deflections and the dimensionless stresses (normal and transverse shear) of the square FG plate ($a/h = 10$ and $a = b$) for different values of the volume fraction P. The present predictions (present high-order theory) are compared with those obtained using the first-order (FSDPT) [62], parabolic (PSDPT) [49], and sinusoidal (SSDPT) shear deformation theories [61]. Table 2 includes the porosity factor α.

It should be noted that all theories (FSDPT, PSDTT and SSDPT) were obtained based on the sinusoidal variation of both in-plane and transverse displacements across the thickness. It can be seen that SSDPT presented sinusoidal theory with five unknowns. The present results in the non-porous case ($\alpha = 0$) are almost more accurate than those obtained using other theories. Also, the present results are satisfactorily compared with other solutions, even for thicker plates. This evidences that the use of new assumption given in Eq. (6) has a maximal effect on the accuracy of the results. The stresses are compared with those of other theories. Generally, the present theory (with $\alpha = 0$) gives a good prediction of in-plane normal stress as compared with different models (PSDTT and SSDPT). However, the transverse normal stress is in good agreement with the SSDPT solution.

Finally, additional results of deflections, normal stresses and transverse shear stresses are reported in Tables 3, 4, and 5, respectively, for porous and non-porous FG plates ($\alpha = 0$, 0.1, 0.2, and 0.3). The inclusion of porosity parameter increases the deflection and the transverse shear stresses, and decreases the axial stress for different values of the volume-fraction-graded-factor P.

Fig. 2 shows the increase in dimensionless displacements, which is explained by the influence of material stiffness, i.e. an increase in the value of porosity (α) leads to a decrease in the modulus of elasticity of the plate. An increase in the side-to-thickness ratios (a/h) leads to an increase in the adimensional displacements. We can also say that the thickness ratio (a/h) has a considerable effect on the dimensionless displacement.

In Fig. 3, we study the variations of the adimensional displacement as a function of the geometric ratio (a/b) for different values of the porosity coefficient with a ratio of equal thickness ($a/h = 10$) and a material index $P = 2$. In addition, the deflection of the non-porous (α) and non-porous ($\alpha = 0$) FG plate decreases as the aspect ratio increases, whereas it may be unchanged as the side-to-thickness ratio increases.

Table 3
Effects of the volume fraction and porosity coefficient of deflections in a square FG plate.

P	$\alpha = 0.0$	$\alpha = 0.1$	$\alpha = 0.2$	$\alpha = 0.3$
Ceramic	0.07790	0.08122	0.08482	0.08877
1	0.19604	0.21876	0.24749	0.28499
2	0.28479	0.33573	0.40910	0.52402
3	0.33606	0.40946	0.52436	0.73018
4	0.36452	0.45243	0.59694	0.87922
5	0.38090	0.47780	0.64172	0.97968
Metal	0.42290	0.34624	0.29310	0.25410

Table 4
Effects of the volume fraction and porosity coefficient on the dimensionless axial stress in a square FG plate.

P	$\alpha = 0.0$	$\alpha = 0.1$	$\alpha = 0.2$	$\alpha = 0.3$
Ceramic	1.99550	1.99550	1.99550	1.99550
1	0.94407	0.82120	0.66571	0.46260
2	1.37702	1.26609	1.10626	0.85584
3	1.62591	1.54558	1.41992	1.19499
4	1.76267	1.70732	1.61657	1.43973
5	1.84026	1.80177	1.73700	1.60414
Metal	1.99550	1.99550	1.99550	1.99550

Table 5
Effects of volume fraction and porosity coefficient on the dimensionless transverse shear stresses in a square FG-plate.

P	$\alpha = 0.0$	$\alpha = 0.1$	$\alpha = 0.2$	$\alpha = 0.3$
Ceramic	0.24618	0.24618	0.24618	0.24618
1	0.34103	0.34764	0.35539	0.36466
2	0.41426	0.42864	0.44641	0.46953
3	0.47502	0.49672	0.52408	0.56107
4	0.52827	0.55720	0.59391	0.64400
5	0.57591	0.61219	0.65850	0.72175
Metal	0.24618	0.24618	0.24618	0.24618

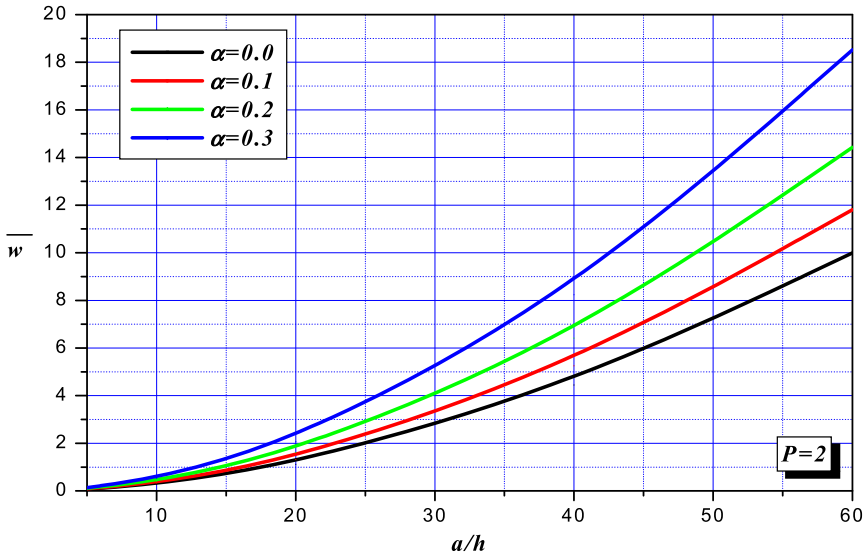

Fig. 2. Variation of the dimensionless displacement as a function of the thickness ratio a/h for different values of the porosity factor α.

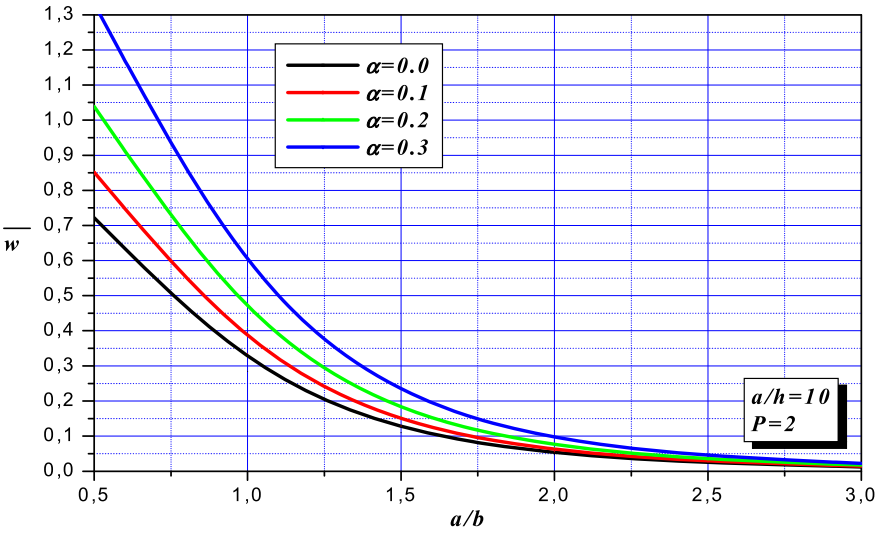

Fig. 3. Variation of the adimensional displacement as a function of the geometric ratio a/b for different values of the porosity factor α.

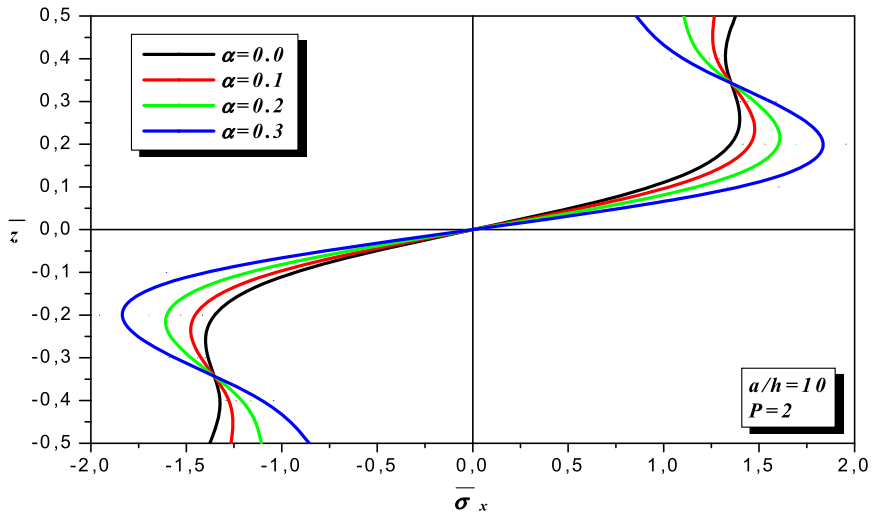

Fig. 4. Through-the-thickness distribution of the axial stress $\overline{\sigma}_x$ of the FGM plates for different values of the porosity factor α.

Fig. 4 displays the variation of the axial stress across the plate thickness in FGM. The effect of the porosity of the FGM plate was taken into account by means of the introduction of coefficient α. Four values are therefore retained ($\alpha = 0$, 0.1, 0.2, and 0.3). It can be seen that an increase in the index of porosity (α) leads to an increase in stress. This can be justified by the fact that the porosity reduces the rigidity of the plate. The stresses are tensile above the median plane and compressive below the median plane. It is important to observe that the maximum stress depends on the value of the exponent of the volume fraction P.

Shear stresses are plotted through the transverse thickness distribution in Fig. 5. It can be seen from this figure that the porosity effect has a remarkable direct influence starting at a point on the median plane of the FG plate, which decreases the transverse shear stress.

8. Conclusions

A new simple theory of high-order shear and normal deformation theory is developed for ceramic/metal functionally graded plates. This theory satisfies the nullity of the stresses at the upper and lower surfaces of the plate without using the shear correction factor, contrary to other theories. The law of the modified mixture covering the porosity phases is used to roughly describe the variations with porosity of the properties of FG plates. The effects of various parameters, such as thickness ratio, gradient index, and volume fraction of porosity on the flexion of FG ceramic–metal plates are all discussed. Many validation examples are reported, and the numerical results obtained with the present high-order shear plate theory are accurate for predicting the static analysis of non-porous plates. In addition, the present theory gave control results that

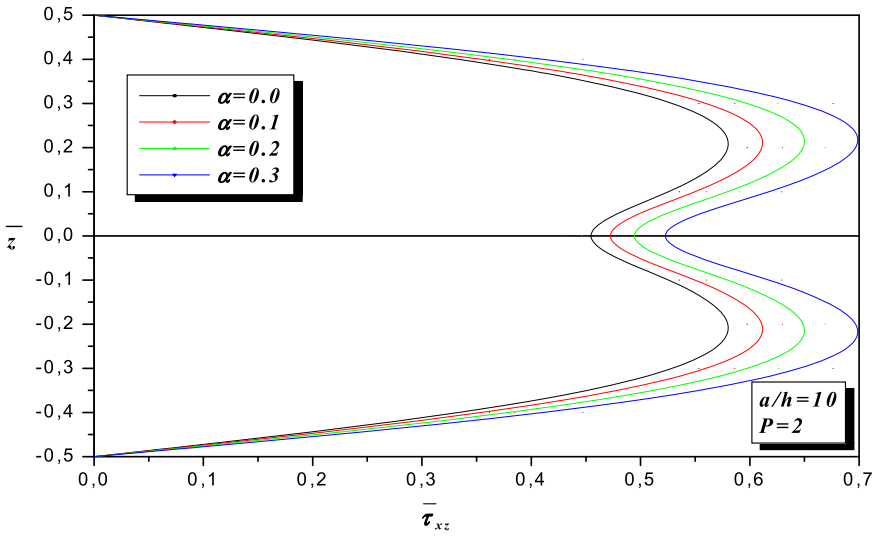

Fig. 5. Through-the-thickness distribution of transverse shear stress $\overline{\tau}_{xz}$ of FGM plates for different values of the porosity factor α.

can be used to evaluate various plate theories, and also to compare the results of the latter with the those obtained by other methods (FSDPT, PSDPT and SSDPT). From this work, it can be inferred that the present theory is a simple allowing one to solve the problem of the mechanical behavior of FG plates with porosity caused by press manufacturing defects.

References

[1] S. Suresh, A. Mortensen, Fundamental of Functionally Graded Materials, Maney, London, 1998.
[2] J. Zhu, Z. Lai, Z. Yin, J. Jeon, S. Lee, Fabrication of ZrO_2–NiCr functionally graded material by powder metallurgy, Mater. Chem. Phys. 68 (2001) 130–135.
[3] N. Wattanasakulpong, B.G. Prusty, D.W. Kelly, M. Hoffman, Free vibration analysis of layered functionally graded beams with experimental validation, Mater. Des. 36 (2012) 182–190.
[4] A.S. Rezaei, A.R. Saidi, Exact solution for free vibration of thick rectangular plates made of porous materials, Compos. Struct. 134 (2015) 1051–1060.
[5] A. Behravan Rad, M. Shariyat, Three-dimensional magneto-elastic analysis of asymmetric variable thickness porous FGM circular plates with non-uniform tractions and Kerr elastic foundations, Compos. Struct. 125 (2015) 558–574.
[6] A.S. Rezaei, A.R. Saidi, Application of Carrera unified formulation to study the effect of porosity on natural frequencies of thick porous-cellular plates, Composites, Part B, Eng. 91 (2016) 361–370.
[7] N. Shafiei, A. Mousavi, M. Ghadiri, On size-dependent nonlinear vibration of porous and imperfect functionally graded tapered microbeams, Int. J. Eng. Sci. 106 (2016) 42–56.
[8] D. Chen, J. Yang, S. Kitipornchai, Free and forced vibrations of shear deformable functionally graded porous beams, Int. J. Mech. Sci. 108–109 (2016) 14–22.
[9] D. Chen, S. Kitipornchai, J. Yang, Nonlinear free vibration of shear deformable sandwich beam with a functionally graded porous core, Thin-Walled Struct. 107 (2016) 39–48.
[10] F. Ebrahimi, F. Ghasemi, E. Salari, Investigating thermal effects on vibration behavior of temperature-dependent compositionally graded Euler beams with porosities, Meccanica 51 (2016) 223–249.
[11] N. Shafiei, S.S. Mirjavadi, B. MohaselAfshari, S. Rabby, M. Kazemi, Vibration of two-dimensional imperfect functionally graded (2D-FG) porous nano-/micro-beams, Comput. Methods Appl. Mech. Eng. 322 (2017) 615–632.
[12] F. Ebrahimi, A. Jafari, M.R. Barati, Vibration analysis of magneto–electro-elastic heterogeneous porous material plates resting on elastic foundations, Thin-Walled Struct. 119 (2017) 33–46, 2017.
[13] A.S. Rezaei, A.R. Saidi, M. Abrishamdari, M.H. Pour Mohammadi, Natural frequencies of functionally graded plates with porosities via a simple four variable plate theory: an analytical approach, Thin-Walled Struct. 120 (2017) 366–377.
[14] A.S. Rezaei, A.R. Saidi, On the effect of coupled solid–fluid deformation on natural frequencies of fluid saturated porous plates, Eur. J. Mech. A, Solids 63 (2017) 99–109.
[15] B. Lhoucine, E. Khalid, B. Rhali, Thermal behavior analysis at large free vibration amplitudes of thin annular FGM plates with porosities, Proc. Eng. 199 (2017) 528–533.
[16] Y. Wang, D. Wu, Free vibration of functionally graded porous cylindrical shell using a sinusoidal shear deformation theory, Aerosp. Sci. Technol. 66 (2017) 83–91.
[17] M. Ghadiri, H. SafarPour, Free vibration analysis of size-dependent functionally graded porous cylindrical microshells in thermal environment, J. Therm. Stresses 40 (1) (2017) 55–71.
[18] Y.S. Al Rjoub, A.G. Hamad, Free vibration of functionally Euler–Bernoulli and Timoshenko graded porous beams using the transfer matrix method, KSCE J. Civ. Eng. 21 (3) (2017) 792–806.
[19] A. Ghorbanpour Arani, M. Khani, Z. Khoddami Maraghi, Dynamic analysis of a rectangular porous plate resting on an elastic foundation using high-order shear deformation theory, J. Vib. Control. 24 (3) (2017) 1–16.
[20] M.R. Barati, H. Shahverdi, A.M. Zenkour, Electro-mechanical vibration of smart piezoelectric FG plates with porosities according to a refined four-variable theory, Mech. Adv. Mat. Struct. 24 (12) (2017) 987–998.
[21] D. Wu, A. Liu, Y. Huang, Y. Pi, W. Gao, Dynamic analysis of functionally graded porous structures through finite element analysis, Eng. Struct. 165 (2018) 287–301.
[22] E. Arshid, A.R. Khorshidvand, Free vibration analysis of saturated porous FG circular plates integrated with piezoelectric actuators via differential quadrature method, Thin-Walled Struct. 125 (2018) 220–233.

[23] D. Chen, S. Kitipornchai, J. Yang, Dynamic response and energy absorption of functionally graded porous structures, Mater. Des. 140 (2018) 473–487.
[24] M.R. Barati, A general nonlocal stress–strain gradient theory for forced vibration analysis of heterogeneous porous nanoplates, Eur. J. Mech. A, Solids 67 (2018) 215–230.
[25] L. Li, H. Tang, Y. Hu, Size-dependent nonlinear vibration of beam-type porous materials with an initial geometrical curvature, Compos. Struct. 184 (2018) 1177–1188.
[26] M.R. Barati, Vibration analysis of porous FG nanoshells with even and uneven porosity distributions using nonlocal strain gradient elasticity, Acta Mech. 229 (2018) 1183–1196.
[27] F. Ebrahimi, A. Jafari, A four-variable refined shear-deformation beam theory for thermo-mechanical vibration analysis of temperature-dependent FGM beams with porosities, Mech. Adv. Mat. Struct. 25 (3) (2018) 212–224.
[28] M.R. Barati, H. Shahverdi, Nonlinear vibration of nonlocal four-variable graded plates with porosities implementing homotopy perturbation and Hamiltonian methods, Acta Mech. 229 (2018) 343–362.
[29] M. Jabbari, A. Mojahedin, M. Haghi, Buckling analysis of thin circular FG plates made of saturated porous-soft ferromagnetic materials in transverse magnetic field, Thin-Walled Struct. 85 (2014) 50–56.
[30] A.R. Khorshidvand, E. Farzaneh Joubaneh, M. Jabbari, M.R. Eslami, Buckling analysis of a porous circular plate with piezoelectric sensor–actuator layers under uniform radial compression, Acta Mech. 225 (2014) 179–193.
[31] A. Mojahedin, E. Farzaneh Joubaneh, M. Jabbari, Thermal and mechanical stability of a circular porous plate with piezoelectric actuators, Acta Mech. 225 (2014) 3437–3452.
[32] M. Jabbari, M. Hashemitaheri, A. Mojahedin, M.R. Eslami, Thermal buckling analysis of functionally graded thin circular plate made of saturated porous materials, J. Therm. Stresses 37 (2014) 202–220.
[33] E. Farzaneh Joubaneh, A. Mojahedin, A.R. Khorshidvand, M. Jabbari, Thermal buckling analysis of porous circular plate with piezoelectric sensor–actuator layers under uniform thermal load, J. Sandw. Struct. Mater. 17 (1) (2015) 3–25.
[34] M.R. Barati, M.H. Sadr, A.M. Zenkour, Buckling analysis of higher order graded smart piezoelectric plates with porosities resting on elastic foundation, Int. J. Mech. Sci. 117 (2016) 309–320.
[35] A. Mojahedin, M. Jabbari, A.R. Khorshidvand, M.R. Eslami, Buckling analysis of functionally graded circular plates made of saturated porous materials based on higher order shear deformation theory, Thin-Walled Struct. 99 (2016) 83–90.
[36] M.R. Feyzi, A.R. Khorshidvand, Axisymmetric post-buckling behavior of saturated porous circular plates, Thin-Walled Struct. 112 (2017) 149–158.
[37] A.S. Rezaei, A.R. Saidi, Buckling response of moderately thick fluid-infiltrated porous annular sector plates, Acta Mech. 228 (2017) 3929–3945.
[38] P.H. Cong, T.M. Chien, N.D. Khoa, N.D. Duc, Nonlinear thermomechanical buckling and post-buckling response of porous FGM plates using Reddy's HSDT, Aerosp. Sci. Technol. 77 (2018) 419–428.
[39] M.H. Shojaeefard, H.S. Googarchin, M. Ghadiri, M. Mahinzare, Micro temperature-dependent FG porous plate: free vibration and thermal buckling analysis using modified couple stress theory with CPT and FSDT, Appl. Math. Model. 50 (2017) 633–655.
[40] D. Chen, J. Yang, S. Kitipornchai, Nonlinear vibration and postbuckling of functionally graded graphene reinforced porous nanocomposite beams, Compos. Sci. Technol. 142 (2017) 235–245.
[41] S. Kitipornchai, D. Chen, J. Yang, Free vibration and elastic buckling of functionally graded porous beams reinforced by graphene platelets, Mater. Des. 116 (2017) 656–665.
[42] J. Yang, D. Chen, S. Kitipornchai, Buckling and free vibration analyses of functionally graded graphene reinforced porous nanocomposite plates based on Chebyshev–Ritz method, Compos. Struct. 193 (2018) 281–294.
[43] A. Behravan Rad, Static analysis of non-uniform 2D functionally graded auxeticporous circular plates interacting with the gradient elastic foundations involving friction force, Aerosp. Sci. Technol. 76 (2018) 315–339.
[44] E. Reissner, The effect of transverse shear deformation on the bending of elastic plates, Trans. ASME J. Appl. Mech. 12 (1945) 69–77.
[45] R.D. Mindlin, Influence of rotary inertia and shear on flexural motions of isotropic, elastic plates, Trans. ASME J. Appl. Mech. 18 (1951) 31–38.
[46] L. Librescu, On the theory of anisotropic elastic shells and plates, Int. J. Solids Struct. 3 (1967) 53–68.
[47] M. Levinson, An accurate simple theory of the static and dynamics of elastic plates, Mech. Res. Commun. 7 (1980) 343–350.
[48] A. Bhimaraddi, L.K. Stevens, A higher order theory for free vibration of orthotropic, homogeneous and laminated rectangular plates, Trans. ASME J. Appl. Mech. 51 (1984) 195–198.
[49] J.N. Reddy, A simple higher-order theory for laminated composite plates, Trans. ASME J. Appl. Mech. 51 (1984) 745–752.
[50] J.G. Ren, A new theory of laminated plate, Compos. Sci. Technol. 26 (1986) 225–239.
[51] T. Kant, B.N. Pandya, A simple finite element formulation of a higher-order theory for unsymmetrically laminated composite plates, Compos. Struct. 9 (1988) 215–264.
[52] P.R. Mohan, B.P. Naganarayana, G. Prathap, Consistent and variational correct finite elements for higher-order laminated plate theory, Compos. Struct. 29 (1994) 445–456.
[53] A.K. Noor, W.S. Burton, Assessment of shear deformation theories for multilayered composite plates, Appl. Mech. Rev. 42 (1989) 1–13.
[54] J.N. Reddy, A review of refined theories of laminated composite plates, Shock Vib. Dig. 22 (1990) 3–17.
[55] J.N. Reddy, An evaluation of equivalent-single-layer and layerwise theories of composite laminates, Compos. Struct. 25 (1993) 21–35.
[56] M. Mallikarjuna, T. Kant, A critical review and some results of recently developed refined theories of fiber-reinforced laminated composites and sandwiches, Compos. Struct. 23 (1993) 293–312.
[57] L. Dahsin, L. Xiaoyu, An overall view of laminate theories based on displacement hypothesis, J. Compos. Mater. 30 (1996) 1539–1561.
[58] G.N. Praveen, J.N. Reddy, Nonlinear transient thermoelastic analysis of functionally graded ceramic–metal plates, Int. J. Solids Struct. 35 (1998) 4457–4476.
[59] M.M. Najafizadeh, M.R. Eslami, Buckling analysis of circular plates of functionally graded materials under uniform radial compression, Int. J. Mech. Sci. 44 (2002) 2479–2493.
[60] S. Merdaci, A. Tounsi, M.S.A. Houari, I. Mechab, H. Hebali, S. Benyoucef, Two new refined shear displacement models for functionally graded sandwich plates, Arch. Appl. Mech. 81 (2011) 1507e22.
[61] M. Touratier, An efficient standard plate theory, Eng. Sci. 29 (8) (1991) 901–916.
[62] S.P. Timoshenko, J.M. Gere, Mechanics of Materials, D. Van Nostrand Company, New York, 1972.